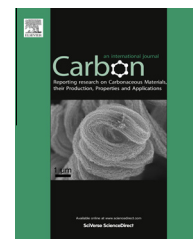


Available at www.sciencedirect.com

SciVerse ScienceDirect

journal homepage: www.elsevier.com/locate/carbon

Nitrogen ion implanted graphene as thrombo-protective safer and cytoprotective alternative for biomedical applications

Meixian Guo ^a, Dejun Li ^{a,*}, Mengli Zhao ^a, Yiteng Zhang ^a, Dongsheng Geng ^b, Andrew Lushington ^b, Xueliang Sun ^b

^a College of Physics and Electronic Information Science, Tianjin Normal University, Tianjin 300387, China

^b Department of Mechanical & Materials Engineering, University of Western Ontario, London, ON, Canada N5X 4J6

ARTICLE INFO

Article history:

Received 20 February 2013

Accepted 4 May 2013

Available online 15 May 2013

ABSTRACT

Nitrogen ion implanted graphene (N/graphene) was investigated for its interaction with mouse fibroblast cells, human endothelial cells and rabbit blood. The results showed that cells cultured on N/graphene displayed increased cell-viability, proliferation, and stretching when compared to those cultured on pristine graphene. An clinical acceptable hemolytic rate (below 5%) and lower platelet adhesion and prolonged kinetic blood-clotting time were also observed for N/graphene, indicating better thromboresistance than pristine graphene. Fourier transformer infrared spectrophotometry (FTIR) and X-ray photoelectron spectroscopy (XPS) measurements proved that N ion implantation induced introduction of N element and appearance of N=C functional groups on N/graphene. The polarity and electronegativity induced by N-containing functional groups on the N/graphene may be related to the improved cytocompatibility and hemocompatibility.

© 2013 Elsevier Ltd. All rights reserved.

1. Introduction

Graphene, a novel carbon-based nanomaterial, has garnered much attention due to its remarkable physical, chemical, and biological characteristics such as high aspect ratio, unique electronic and optical properties, high mechanical strength, as well as its potential biocompatibility. These properties render graphene as an attractive candidate for biomedical applications such as biosensor development, imaging, drug delivery, bacterial inhibition, and photothermal therapy [1–9]. For the purposes of biomedical and clinical applications, however, the preparation of biocompatible graphene is extremely important. In this case, producing a functional graphene becomes crucial.

Some previous works have found that the interaction between multiwalled carbon nanotubes (MWCNTs) and cells was greatly influenced by surface functional groups [10–12].

Carrero-Sanchez et al. demonstrated that MWCNTs chemically doped with nitrogen (CN_x MWCNTs) are more biocompatible when compared with undoped MWCNTs by injecting MWCNTs into mice [10]. Elias et al. took additional biocompatibility tests and supported above results. Their work proved that the validated CN_x MWCNTs were not only innocuous to amoebas but also proliferated in long periods of time and higher CN_x concentrations whereas MWCNTs were lethal [11]. It is therefore believed that CN_x MWCNTs are less harmful than MWNTs and might be more advantageous for bioapplications [11]. In our previous work [12], the improved hemocompatibility and cytocompatibility were also observed in N-doped MWCNTs when compared with pristine MWCNTs using chemical vapor deposition (CVD) method. To graphene, therefore, an appropriate chemical or physical functionalization could also enable it to be well-dispersed in a range of polar solvents, especially water [13,14]. Graphene oxide and functionalized

* Corresponding author. Fax: +86 22 23766519.

E-mail addresses: dejunli@mail.tjnu.edu.cn, dli1961@126.com (D. Li).
0008-6223/\$ - see front matter © 2013 Elsevier Ltd. All rights reserved.
<http://dx.doi.org/10.1016/j.carbon.2013.05.011>

graphene induced by chemical technique have been recently shown to be cytocompatibility for human fibroblast cells and thrombo-protective [15,16]. However, new impurity might be introduced during chemical doping.

Ion implantation is one of the most powerful physical techniques for the surface modification of solids. This technique has many advantages in applications. In addition to the technological simplicity and cleanliness, it modifies only the surface characteristics without affecting bulk properties [17]. It has been applied to the surface modification of polymers in order to control conductivity as well as, mechanical, physical and chemical properties [18–22]. Therefore, if a biomaterial with the desired bulk properties does not exhibit the appropriate biocompatibility, its surface can be modified by ion implantation. To date, N ion implanted graphene (N/graphene) has not been studied for cytocompatibility and hemocompatibility.

In this work, we report, for the first time that positively charged N/graphene is more biocompatible than pristine graphene. Compared with pristine graphene, N/graphene restrains better cytocompatibility for mouse fibroblast cells (L929) and human endothelial cells (EAHY926) and better hemocompatibility for red blood cells, platelets, and blood-clotting times. Thus, N/graphene can be an excellent candidate material for potential biomedical applications in various areas such as imaging, drug delivery, as well as photothermal therapy.

2. Experimental details

2.1. Preparation of samples and characteristic analysis

Graphene powder prepared by modified Hummers' method was dissolved in 1-Methy-2-Pyrrolidinone (NMP) with ultrasonic dispersion for 6 h [23]. The solution was then directly sprayed onto the cycloidal SiO₂ substrates using air brush pistol at 100 °C. Finally, the samples were heated in Ar at 250 °C for 3 h to evaporate NMP. N ion implantation on graphene surface was performed using a BNU-400 kV implanter at room temperature at an energy of 30 keV with a dose of 5×10^{16} ions/cm². Static water contact angles (CA) on pristine graphene and N/graphene were determined using the CAM KSV021733 optical contact-angle inclinometer (Nunc, Finland). High-resolution transmission electron microscopy (HR-TEM) was employed to examine crystallinity and quality of pristine graphene and N/graphene samples. N-containing functional groups and N content of N/graphene was determined by MAGNA-560 fourier transformer infrared (FTIR) spectrophotometer (Nicolet) and Kratos Axis Ultra Al (alpha) X-ray photoelectron spectroscopy (XPS).

2.2. Cell adhesion assays

Biocompatibility assessment of pristine graphene and N/graphene was addressed by culture of the L929 cell line and EAHY926 cell line, which are commonly used to assess cytocompatibility of materials for cell growth, and has been used previously in biocompatibility testing of carbon nanotubes [12]. L929 cells and EAHY926 cells were respectively cultured in Roswell Park Memorial Institute-1640 and

Dulbecco's Modified Eagle Medium High Glucose supplemented with 10% fetal bovine serum, 100 units/ml penicillin and 100 µg/ml streptomycin, in a humidified 5% CO₂ balanced air incubator at 37 °C where the medium was replaced every 2 days. Equal numbers of cells (the inoculum density of EAHY926 and L929 cells were respectively 5×10^4 cells/ml and 1×10^4 cells/ml) were placed in 24 well cell culture plates with the samples. Sterilized samples were incubated with cells in individual wells for 1, 1.5, 2, 3, 5, and 7 days. Cell numbers, after different incubation days, were counted through optical microscopy while trypan blue dye assay was employed to confirm cell viability. Cell morphology and stretching on pristine graphene and N/graphene was observed through the scanning electron microscope (SEM, FEI QUANTA 200).

2.3. Platelet-adhesion assays

Platelet-adhesion testing was performed to investigate the morphology, quantity and aggregation of the adherent platelets on the surfaces of pristine graphene and N/graphene. Fresh blood from healthy rabbit with potassium oxalate as anticoagulant was centrifuged at 1000 r/min about 15 min to prepare Platelets Rich Plasma (PRP). All the samples (including pristine graphene and N/graphene) were placed in the 24-well culture plates and immersed in PRP, after contact with samples at 37 °C for 30 min in water bath. All the samples were fixed in glutaraldehyde and critical-point dry for examination of SEM.

2.4. Hemolysis assays

The diluted blood was obtained by mixing the anticoagulant blood (with 2% potassium oxalate) and normal saline at a volume ratio of 4:5. The pristine graphene and N/graphene were washed three times with normal saline and immersed into 5 ml of normal saline at 37 ± 1 °C for 30 min. 5 ml pure normal saline and pure distilled water (H₂O) were used as negative and positive group respectively. 0.1 ml distilled blood was successively injected into the solution of all groups, gently shaken for uniformity and maintained in a water bath at 37 ± 1 °C for 60 min. The liquid was removed by centrifugation at a rotational speed of 1000 r/min for 10 min. The absorbance value of upper solution was measured at a wavelength of 540 nm with a spectrophotometer. The optical density (O.D.) is related to the concentration of free hemoglobin in the supernatant due to broken red blood cells. The hemolysis ratio is calculated by the formula:

$$\text{Hemolytic rate(\%)} = \frac{A - B}{C - B} \times 100\%$$

where A, B and C respectively stand for the O.D. values of measured samples, the negative control group (normal saline), and the positive control group (H₂O).

2.5. Kinetic blood-clotting time assays

0.1 ml fresh blood taken from a healthy adult rabbit was dropped onto the surface of pristine graphene and N/graphene. After being kept for 5 min, 10 min, 20 min, 30 min, 40 min, 50 min respectively, the samples were trans-

ferred into a beaker and 50 ml distilled water was added into the beaker. Then the escaped erythrocytes from thrombus were hemolytic, and the freed hemoglobin was dispersed in the solution. The concentration of freed hemoglobin in the solution was colorimetrically measured by a spectrophotometer at a wavelength of 540 nm. The O.D. at 540 nm ($O.D._{540\text{ nm}}$) of the solution vs. time was plotted. Generally $O.D._{540\text{ nm}}$ value decreases with blood clotting.

3. Results and discussion

HR-TEM images of pristine graphene and N/graphene are shown in Fig. 1a and b. Compared with pristine graphene, N/graphene displays the planar graphene clearly, indicating that N ion implantation results in higher surface/volume ratio. The contact angles of pristine graphene and N/graphene are $89.54 \pm 2^\circ$ and $81.48 \pm 2^\circ$ respectively. A slight improvement in wettability for N/graphene may be related to appearance of N-containing polar groups caused by N ion implantation, which will be proved by following measurements. Wettable surfaces can promote fibronectin adsorption which is consistent with cell proliferation, migration, differentiation and apoptosis. Otherwise, nonwetable surfaces with low surface energy can result in protein denaturation. Whereas the inner hydrophobic residues of proteins in turn prevents specific interactions to occur between the adsorbed protein and cells [24,25]. So, a slight increase in wettability is beneficial to cell adhesion and growth for N/graphene.

Furthermore, analysis of binding energy (BE) values in XPS spectra of C1s (Fig. 2b and c) indicates further evidence of the existence of the unique C=N functional groups induced by N ion implantation. The pristine graphene and N/graphene are further characterized by the appearance of several spectral peaks: C–C and/or C=C at 284.7 eV, C=N at 285.7 eV and C=O 288.2 eV. It is obviously that the peak of C=N increases after N ion implantation, as N content increases from 0.91 atm.% to 2.31 atm.%. Whereas the disappearance of C=O peak after N ion implantation reveals the cleavage of some pendant such as O-containing groups after N ion implantation. Based on the detailed analysis of N1s (Fig. 2d), nitrogen peaks in the spectrum of N/graphene are observed at BE = 398.1 eV for pyridinic N, BE = 399.9 eV for pyrrolic N and BE = 401.3 eV for quaternary N [26]. The presence of these

different types of nitrogen in graphitic network is possible to activate the growth and proliferation of cells. It is also less injurious to living organism. We believe that N-containing functional group on the surface induced by N ion implantation is the main reason for the improved biocompatibility for N/graphene when compared with pristine graphene.

Due to the novelty of N/graphene, its biocompatibility is relatively unknown. Vitro cell culture is conducted in order to determine its cytocompatibility. L929 cell lines are selected based on recommendations outlined by the International Standard Organization (ISO) committee as an *in vitro* biocompatibility test model [27]. The number of alive L929 cells that are exposed to N/graphene and pristine graphene with incubation time is summarized in Fig. 3. Each value in this figure represents the mean \pm SD for five measurements. Each experiment is performed three times. From 1 to 5 days, the concentration of cells on pristine graphene increases gradually. After 5 days, however, the cell numbers steadily reduce. In contrast, the cell concentration on N/graphene consistently increases until 7th day. At the 7th day, L929 cell numbers on N/graphene outdistance that on pristine graphene. After 7 days, the cell apoptosis starts. This indicates that the cell apoptosis on N/graphene delays two days compared to that on pristine graphene. At the 9th day, the majority of cells are apoptosis due to the growth of limited space. This indicates that N ion implantation leads graphene to provide a better growth environment for cell viability than pristine graphene. From 1 to 3 days, no dead cells are observed under optical microscope for both samples. After 5 days incubation, the percentage of the dead cell numbers from N/graphene is lower than 10%, whereas the percentage of the dead cell numbers from pristine graphene is up to 18%. This implies the significant contributions of N-containing functional groups to cellular tissues and the voile-like structures consisting of randomly crumpled sheets, which offers polar surface and larger substrate area for cell growth and proliferation.

Cytocompatibility assessment of pristine graphene and N/graphene is also addressed by culture of the human endothelial cells (EAHY926). To investigate EAHY926 cells viability on the samples, the cell number on pristine graphene and N/graphene are counted after 1–7 days of incubation, as shown in Fig. 4. The cell growth shows a slow increase across the 7 day period for pristine graphene. Compared with the

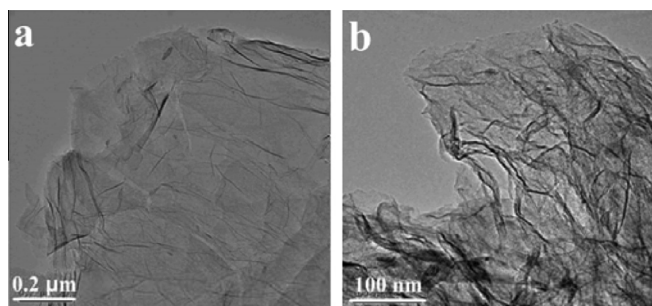


Fig. 1 – HR-TEM images of pristine graphene (a) and N/graphene (b) FTIR is performed to analyze the changes of the functional groups caused by N ion implantation (Fig. 2a). C–C bonds are observed at the wave number of 1110 cm^{-1} for pristine graphene and N/graphene. However a unique C=N bond appeals in N/graphene at the wave number of 1260 cm^{-1} , indicating that N ion implantation successfully introduces N-containing functional groups to the surface of graphene.

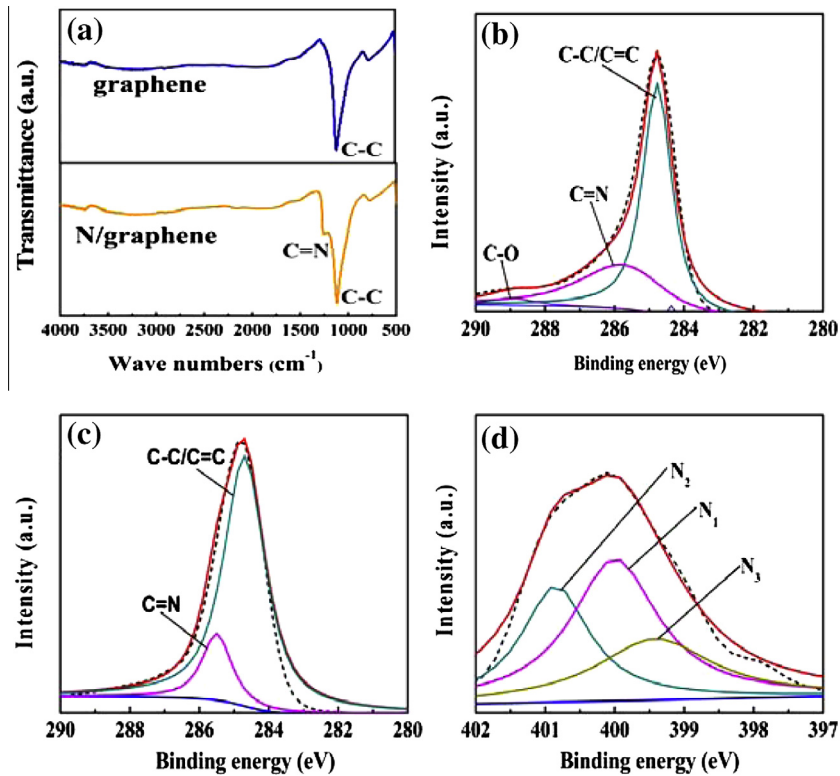


Fig. 2 – FTIR spectra obtained from pristine graphene and N/graphene (a); XPS C1s spectra of pristine graphene (b) and N/graphene (c); N1s spectrum of N-graphene (d) with N1 (pyrrole-like N), N2 (quaternary N), and N3 (pyridine-like N).

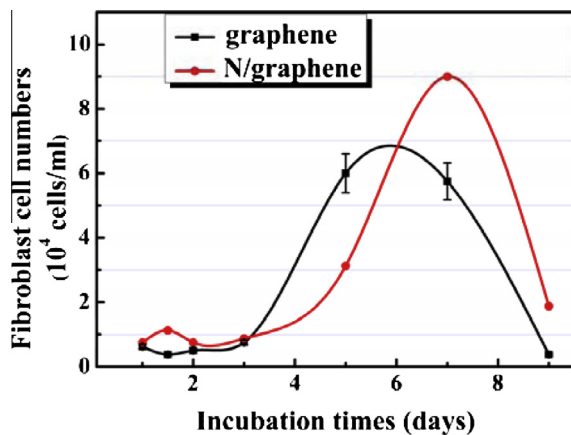


Fig. 3 – L929 fibroblast cell numbers on the surfaces of pristine graphene and N/graphene.

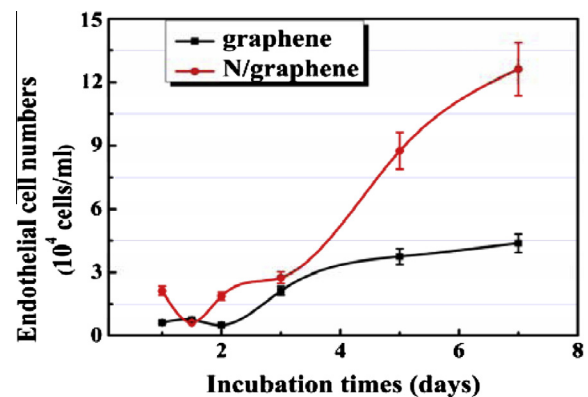


Fig. 4 – EAHY926 endothelial cell numbers on the surfaces of pristine graphene and N/graphene.

low number and low viability of the cells on pristine graphene, N/graphene displays high cell number and rapid proliferation. These results provide further evidence for the enhanced cytocompatibility of N/graphene.

The morphologies of L929 cells and EAHY926 cells on the surfaces of pristine graphene and N/graphene after 48 h of incubation are showed by SEM in Figs. 5 and 6. It is obvious that cells on the surface of pristine graphene for 48 h of incubation (Figs. 5a and 6a) show irregular, spindly, detaching from culture plates. Figs. 5c and 6c further indicate that L929 and EAHY926 cell surfaces are covered a layer of secretion, which might be due to the mutation and coalescence

of the membrane protein induced by cellular metabolism and apoptosis [28,29]. Whereas cells adhered to the surface of the N/graphene (Figs. 5b and 6b) reveal typical appanate states and have a significant tendency to attach to the substrate and intersect with pseudopod. The cell size on N/graphene is larger than one on pristine graphene. The cells completely extend and occupy the entire visual area, indicating a significant improvement in cell attachment and growth on N/graphene. Figs. 5d and 6d further show that the cells spread obviously and form visible lamellipodia, indicating cell growth becomes faster as incubation time.

This result demonstrates that the N/graphene can provide a proper surface for normal cellular attachment and growth.

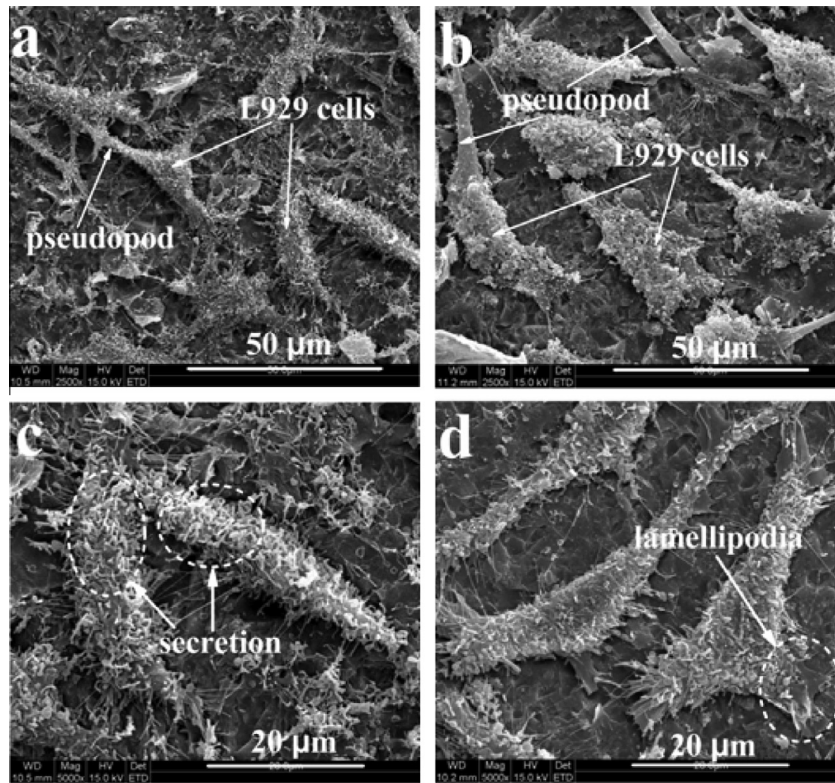


Fig. 5 – SEM images of L929 fibroblast cells on pristine graphene (a, c) and N/graphene (b, d).

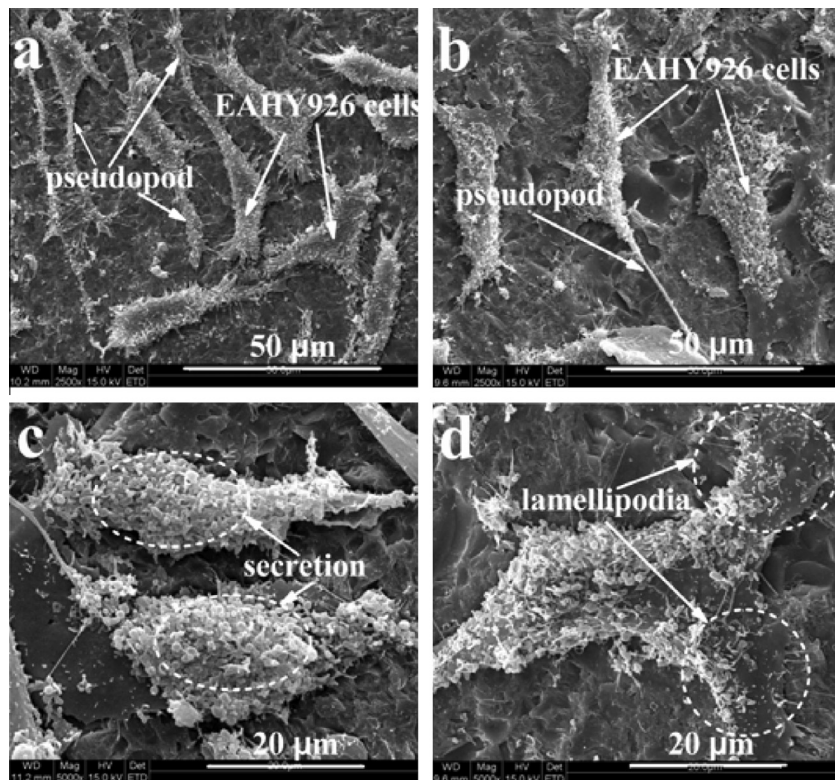


Fig. 6 – SEM images of EAHY926 endothelial cells on pristine graphene (a, c) and N/graphene (b, d).

A possible mechanism is due to nonspecific binding that occurs between nitrogen in N-containing functional groups on

N/graphene and cell-surface proteins enhance cell adhesion and growth. The ability of cells adhesion on substrates de-

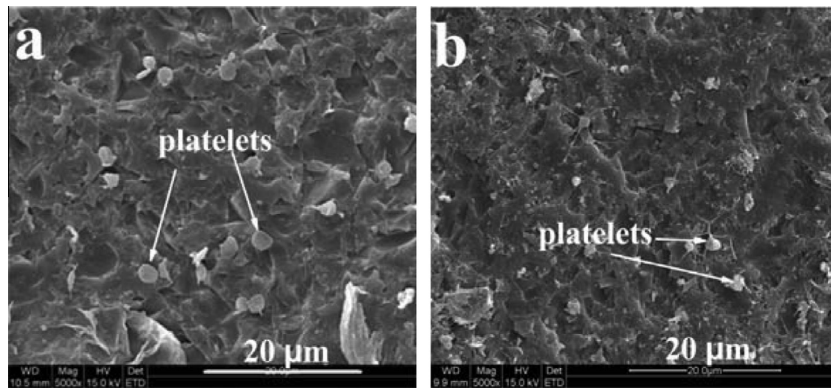


Fig. 7 – SEM images of the platelets on pristine graphene (a) and N/graphene (b).

depends on the interaction of adsorbed proteins from the culture medium and the receptors on the cell surface. Thus, polar functional groups of N/graphene act as a site for the cell growth. N ion implantation leads to polarization of N/graphene owing to the difference in electronegativity between carbon and nitrogen. The polarization as well as unsaturated degree of N bonds promotes protein attachment on the material's surface, improving cytocompatibility.

Surface wettability is affected not only by surface chemistry but also by topographical parameters such as roughness and texture. These characteristics may affect the proliferation of cells due to an initial phase of attachment that involves a physicochemical linkage to occur between cells and surfaces either through interfaces or indirectly through an alteration in the adsorption of conditioning molecules such as proteins [30]. As direct interaction between nanomaterials and cells modulates critical cell signalling pathways and contributes to observed toxicity, N ion implantation results in the modification of surface charge with ensuing diminished effect on nanomaterial-cell interaction and can bring about significant attenuation in toxicity.

Platelet activation plays a critical role in thrombus cascade reactions. Monitoring of the platelet behavior is a common

hemocompatibility evaluation method. The SEM images of platelets adhering onto surfaces of the substrates are presented in Fig. 7. It can be seen from SEM images that slight more platelets exists on pure graphene surface than N/graphene, which indicates better anticoagulation for N/graphene. Thrombogenicity occurring on foreign material surface in contact with blood is a complicated process. The polar surface has a positive effect on the platelet adhesion and activation. Therefore, the existence of N-containing functional groups induced by N ion implantation leads N/graphene to polarity and high electronegativity, which should be responsible for enhanced thromboresistance.

Optical Density is often related to the concentration of free hemoglobin in the supernatant due to broken red blood cells. In this assay centrifugation of the positive group (H₂O) results in a red supernatant (inset A in Fig. 8) due to a large amount of hemoglobin released from broken red blood cells as a consequence of osmotic shock. However, pure graphene and N-graphene (inset B, C in Fig. 8) show transparent supernatants like the negative control group (inset D in Fig. 8), because most of red blood cells are undamaged and settled down to the bottom of the tube.

Fig. 8 shows the hemolytic-rate results of pristine graphene and N/graphene. Both samples have a hemolytic rate

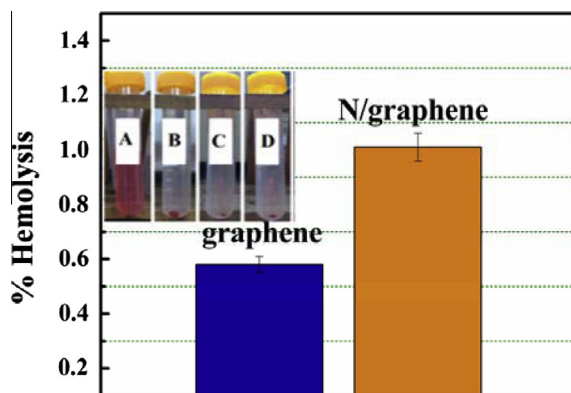


Fig. 8 – Hemolytic rates of pristine graphene and N/graphene. The inset A, B, C, D are the supernatants containing the positive group (H₂O), pristine graphene, N/graphene, and the negative control group (normal saline).

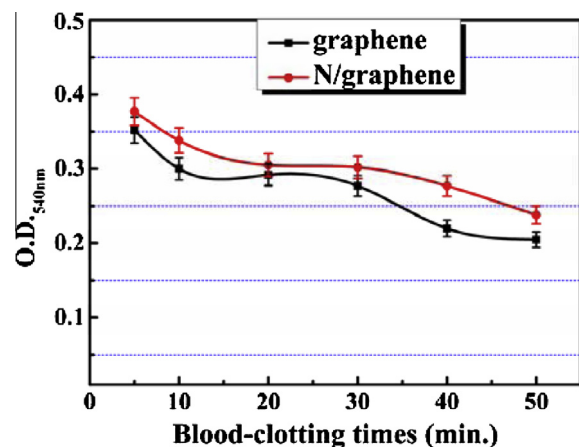


Fig. 9 – The O.D._{540 nm} values of pristine graphene and N/graphene vs. blood-clotting time.

far lower than the YY/T0127.1 standard or clinical acceptable value of 5% [31,32], indicating that graphene before and after functionalization are nonhemolytic.

The O.D. of the hemolyzed hemoglobin solution changes with time. The higher the optical density, the better the thromboresistance is. When the blood is completely clotted on the sample, the O.D._{540 nm} value of the solution decreases to a steady range. Generally, blood start to clot occurs at O.D._{540 nm} of 0.1 value at which the kinetic blood-clotting time on the sample surfaces is recorded. From Fig. 9, it is clear that the curve of optical density vs. the clotting time for N/graphene is always upper than that for pristine graphene, which implies that N/graphene has slight better the thromboresistance than pristine graphene.

4. Conclusions

Functionalization of graphene is successfully attained by N ion implantation while microstructure and bonding are systematically investigated. The cytocompatibility and hemocompatibility of pristine graphene and N/graphene are investigated and compared in detail. L929 and EAHY926 cells are adhered onto pristine graphene and N/graphene to form an expanding population of polygonal cells. N/graphene exhibits higher cell-adhesion strength, cell viability, cell proliferation and cell stretching. No obvious toxicity is observed on N/graphene. The blood assays also indicate that N/graphene has slightly lower platelet adhesion and prolonged kinetic blood-clotting time than pristine graphene. The existence of N-containing functional groups induced by N ion implantation produces high polarity and electronegativity, which might be main reasons for enhanced cytocompatibility and hemocompatibility. The improved biocompatibility of N/graphene remains a challenge for use of this novel material in biomedical application. Further work will focus on investigating the possible mechanism of interaction between N/graphene and cells and protein.

Acknowledgements

This work was supported by National Natural Science Foundation of China (51272176, 11075116), National Basic Research Program of China (973 Program, 2012CB933600).

REFERENCES

- [1] Wang Y, Li YM, Tang LH, Lu J, Li JH. Application of graphene-modified electrode for selective detection of dopamine. *Electrochem Commun* 2009;11(4):889–92.
- [2] Liu Y, Yu D, Zeng C, Miao Z, Dai L. Biocompatible graphene oxide-based glucose biosensors. *Langmuir* 2010;26(9):6158–60.
- [3] Peng C, Hu W, Zhou Y, Fan C, Huang Q. Intracellular imaging with a graphene-based fluorescent probe. *Small* 2010;6(15):1686–92.
- [4] Sun XM, Liu Z, Welsher K, Robinson JT, Goodwin A, Zaric S, et al. Nano-graphene oxide for cellular imaging and drug delivery. *Nano Res* 2008;1(3):203–12.
- [5] Liu Z, Robinson JT, Sun XM, Dai H. PEGylated nanographene oxide for delivery of water-insoluble cancer drugs. *J Am Chem Soc* 2008;130(33):10876–7.
- [6] Hu WB, Peng C, Luo WJ, Lv M, Li XM, Li D, et al. Graphene-based antibacterial paper. *ACS Nano* 2010;4(7):4317–23.
- [7] Akhavan O, Ghaderi E. Toxicity of graphene and graphene oxide nanowalls against bacteria. *ACS Nano* 2010;4(10):5731–6.
- [8] Yang K, Zhang S, Zhang GX, Sun XM, Lee ST, Liu Z. Graphene in mice: ultrahigh in vivo tumor uptake and efficient photothermal therapy. *Nano Lett* 2010;10(9):3318–23.
- [9] Robinson JT, Tabakman SM, Liang Y, Wang HL, Casalongue HS, Vinh D, et al. Ultra small reduced graphene oxide with high near-infrared absorbance for photothermal therapy. *J Am Chem Soc* 2011;133(17):6825–31.
- [10] Carrero-Sainchez JC, Elias AL, Mancilla R, Arrellin G, Terrones H, Laclette JP, et al. Biocompatibility and toxicological studies of carbon nanotubes doped with nitrogen. *Nano Lett* 2006;6(8):1609–16.
- [11] Ana LE, Julio CCS, Humberto T, Morinobu E, Juan PL, Mauricio T. Viability studies of pure carbon- and nitrogen-doped nanotubes with entamoeba histolytica: from amoebicidal to biocompatible structures. *Small* 2007;3(10):1723–9.
- [12] Zhao ML, Li DJ, Yuan L, Yue YC, Liu H, Sun XL. Differences in cytocompatibility and hemocompatibility between carbon nanotubes and nitrogen-doped carbon nanotubes. *Carbon* 2011;49:3125–33.
- [13] Shan CS, Yang HF, Han DX, Zhang QX, Ivaska A, Niu L. Water-soluble graphene covalently functionalized by biocompatible Poly-L-Lysine. *Langmuir* 2009;25(20):12030–3.
- [14] Luo JY, Cote LJ, Tung VC, Tan ATL, Goins PE, Wu J, et al. Graphene oxide nanocolloids. *J Am Chem Soc* 2010;132(50):17667–9.
- [15] Singh SK, Singh MK, Kulkarni PP, Sonkar VK, Gracio JJA, Dash D. Amine-modified graphene: thrombo-protective safer alternative to graphene oxide for biomedical applications. *ACS Nano* 2012;6(3):2731–40.
- [16] Lee HJ, Park J, Yoon OJ, Kim HW, Lee DY, Kim DH, et al. Amine-modified single-walled carbon nanotubes protect neurons from injury in a rat stroke model. *Nat Nanotechnol* 2011;6:121–5.
- [17] Li DJ, Cui FZ, Gu HQ. F ion implantation induced cell attachment on intraocular lens. *Biomaterials* 1999;20(20):1889–96.
- [18] Venkatesan T, Dynes RC, Wilkens B, White AE, Gibson JM, Hamm R. Comparison of conductivity produced in polymers and carbon films by pyrolysis and high energy ion irradiation. *Nucl Instrum Meth B* 1984;1(2–3):599–604.
- [19] Koh SK, Choi KW, Cho JS, Song SK, Kim YM, Jung HJ. Ar⁺ ion irradiation in oxygen environment for improving wettability of polymethylmethacrylate. *J Mater Res* 1996;11(11):2933–9.
- [20] Wang GH, Pan GQ, Dou L. Proton beam modification of isotactic polypropylene. *Nucl Instrum Meth B* 1987;27(3):410–6.
- [21] Wang GH, Li XJ, Zhu YZ, Liu QS, Hu NX, Gu XS, et al. Radiation effects on polyethylene and polypropylene by electrons and protons. *Nucl Instrum Meth B* 1985;7(8):497–500.
- [22] Licciardello A, Fragala ME, Foti G, Compagnini G, Puglisi Q. Ion beam effects on the surface and on the bulk of thin films of polymethylmethacrylate. *Nucl Instrum Meth B* 1996;116(1–4):168–72.
- [23] Geng DS, Yang SL, Zhang Y, Yang JL, Liu J, Li RY, et al. Nitrogen doping effects on the structure of graphene. *Appl Surf Sci* 2011;257:9193–8.
- [24] Grinnel F, Feld MK. Fibronectin adsorption on hydrophilic and hydrophobic surfaces detected by antibody binding and

- analyzed during cell adhesion in serum-containing medium. *J Biol Chem* 1982;257(9):4888–93.
- [25] Lu DR, Park K. Effect of surface hydrophobicity on the conformational changes of adsorbed fibrinogen. *J Colloid Interface Sci* 1991;144(1):271–81.
- [26] Geng DS, Yang SL, Zhang Y, Yang JL, Liu J, Li RY, et al. Nitrogen doping effects on the structure of graphene. *Appl Surf Sci* 2011;257:9193–8.
- [27] Zange R, Kissel T. Comparative in vitro biocompatibility testing of polycyanoacrylates and poly(D, L-lactide-co-glycolide) using different mouse fibroblast (L929) biocompatibility test models. *Eur J Pharm Biopharm* 1997;44(2):149–57.
- [28] Abhilash S, Leela SP, Aparna RS, Anusha A, Parwathy C, Chundayil MG, et al. Hemocompatibility and macrophage response of pristine and functionalized graphene. *Small* 2012;8(8):1251–63.
- [29] Li Y, Liu Y, Fu Y, Wei T, Guyader LL, Gao G, et al. The triggering of apoptosis in macrophages by pristine graphene through the MAPK and TGF-beta signaling pathways. *Biomaterials* 2012;33(2):402–11.
- [30] Akasaka T, Yokoyama A, Matsuoka M, Hashimoto T, Watari F. Thin films of single-walled carbon nanotubes promote human osteoblastic cells (Saos-2) proliferation in low serum concentrations. *Mater Sci Eng C* 2010;30:391–9.
- [31] Gao JC, Li LC, Wang Y, Qiao LY. Corrosion resistance of alkali heat treated magnesium in bionics simulated body fluid. *Rare Metal Mat Eng* 2005;30:903–7.
- [32] Alanazi A, Hirakuri KK. Blood compatibility of DLC films. *Eur Cells Mater* 2010;20(1):15–20.